

# Total Molecular Gas Masses of *Planck* – *Herschel* Selected Strongly Lensed Hyper Luminous Infrared Galaxies

K. C. Harrington<sup>1,2\*</sup>, M. S. Yun<sup>3</sup>, B. Magnelli<sup>2</sup>, D.T. Frayer<sup>4</sup>,  
A. Karim<sup>2</sup>, A. Weiß<sup>1</sup>, D. Riechers<sup>5</sup>, E. F. Jiménez-Andrade<sup>1,2</sup>, D. Berman<sup>3</sup>,  
J. Lowenthal<sup>6</sup>, and F. Bertoldi<sup>2</sup>

<sup>1</sup>Max-Planck-Institut für Radioastronomie, Auf dem Hügel 69, 53121 Bonn, Germany

<sup>2</sup>Argelander Institut für Astronomie, Auf dem Hügel 71, 53121 Bonn, Germany

<sup>3</sup>Department of Astronomy, University of Massachusetts, 619E Lederle Grad Research Tower, 710 N. Pleasant Street, Amherst, MA 01003, USA

<sup>4</sup>Green Bank Observatory, 155 Observatory Rd., Green Bank, West Virginia 24944, USA

<sup>5</sup>Department of Astronomy, Cornell University, Space Sciences Building, Ithaca, NY 14853, USA

<sup>6</sup>Department of Astronomy, Smith College, Northampton, MA 01063, USA

28 September 2018

## ABSTRACT

We report the detection of CO(1 – 0) line emission from seven *Planck* and *Herschel* selected hyper luminous ( $L_{\text{IR}(8-1000\mu\text{m})} > 10^{13}L_{\odot}$ ) infrared galaxies with the Green Bank Telescope (*GBT*). CO(1 – 0) measurements are a vital tool to trace the bulk molecular gas mass across all redshifts. Our results place tight constraints on the total gas content of these most apparently luminous high- $z$  star-forming galaxies (apparent IR luminosities of  $L_{\text{IR}} > 10^{13-14}L_{\odot}$ ), while we confirm their predetermined redshifts measured using the Large Millimeter Telescope, *LMT* ( $z_{\text{CO}} = 1.33 - 3.26$ ). The CO(1 – 0) lines show similar profiles as compared to  $J_{\text{up}} = 2 - 4$  transitions previously observed with the *LMT*. We report enhanced infrared to CO line luminosity ratios of  $\langle L_{\text{IR}}/L'_{\text{CO}(1-0)} \rangle = 110 \pm 22 L_{\odot}(\text{K km s}^{-1} \text{pc}^{-2})^{-1}$  compared to normal star-forming galaxies, yet similar to those of well-studied IR-luminous galaxies at high- $z$ . We find average brightness temperature ratios of  $\langle r_{21} \rangle = 0.93$  (2 sources),  $\langle r_{31} \rangle = 0.34$  (5 sources), and  $\langle r_{41} \rangle = 0.18$  (1 source). The  $r_{31}$  and  $r_{41}$  values are roughly half the average values for SMGs. We estimate the total gas mass content as  $\mu M_{\text{H}_2} = (0.9 - 27.2) \times 10^{11}(\alpha_{\text{CO}}/0.8)M_{\odot}$ , where  $\mu$  is the magnification factor and  $\alpha_{\text{CO}}$  is the CO line luminosity to molecular hydrogen gas mass conversion factor. The rapid gas depletion times,  $\langle \tau_{\text{depl}} \rangle = 80$  Myr, reveal vigorous starburst activity, and contrast the Gyr depletion timescales observed in local, normal star-forming galaxies.

**Key words:** galaxies: high-redshift – galaxies: starburst – submillimeter: galaxies – galaxies: ISM – gravitational lensing: strong

## 1 INTRODUCTION

Most of the stars in the local universe formed out of tremendous cool gas reservoirs ( $M_{\text{gas}} \sim 10^{10-11}M_{\odot}$ ,  $T \sim 10 - 100$  K) in the interstellar medium (ISM) of high redshift ( $1 < z < 3.5$ ) galaxies with intense star-formation (SF) (Carilli & Walter 2013; Madau and Dickinson, 2014).

Massive, dusty star forming galaxies at high- $z$  (DSFGs;  $M_{\text{dust}} \sim 10^{8-9}M_{\odot}$ ) are typically gas-rich galaxies selected via their bright observed (sub)-mm fluxes (also known as SMGs). The rest-frame far-IR (FIR)-mm luminosity associ-

ated with the thermal dust emission (Efstathiou et al. 2000; Johnson et al. 2013) (re-radiated far-UV radiation) traces the total star-formation (SF) activity, while the extreme star-formation rates (SFRs) in these IR luminous galaxies are likely due to a sustained supply of cool gas from the intergalactic medium (IGM). The dense molecular ingredients of the ISM thereby limits the timescale for extended starburst (SB) activity, with short-lived SB episodes of 10's-100's of Myr. These are believed to often include gas-rich mergers that induce star formation via tidal torques, which drive gas infall and subsequent collapse (Hernquist 1992). The most active SB galaxies at  $z \sim 2$  contribute key insights into galaxy evolution and structure formation, as their mas-

\* E-mail: kharring@astro.uni-bonn.de

sive gas reservoirs play a key role in the bulk stellar mass growth in their ISM environments, and as a result are believed to be the progenitors to massive elliptical/spheroidal galaxies and clusters at low- $z$  (Casey et al. 2014).

The SMG population can be accounted for by major or minor-merger dominated starbursts (Baugh et al. 2005; Swinbank et al. 2008) in some semi-analytic models. Others suggest that the observed population is a heterogeneous mix of early and late stage major mergers and blending of passive star-forming disc galaxies. The brightest SMGs are likely early-stage mergers, exchanging a significant amount of molecular material for continued star formation (Hayward et al. 2012; Narayanan et al. 2015). SMGs typically have high gas mass fractions,  $M_{\text{gas}}/M_*$ , up to 80% (Carilli & Walter 2013).

CO line measurements are vital for directly probing the fuel for these star-forming galaxies, i.e. the total molecular gas mass, at the peak of the co-moving SFR density ( $z \sim 2 - 3$ ). The gas accretion history of growing dark matter (DM) halos in cosmological simulations (Kereš et al. 2005) agrees well with the observed evolution of the CO luminosity function, as Decarli et al. (2016a) find a peak redshift for CO luminous galaxies at  $z \sim 2$ , comparable to the peak of the co-moving star formation rate density.

The CO ( $J=1 \rightarrow 0$ ) transition accounts for both the dense and most diffuse molecular gas, and has traditionally been calibrated to trace the bulk  $\text{H}_2$  gas mass (via collisional excitation with the  $\text{H}_2$  gas). The observed CO line luminosity,  $L'_{\text{CO}}$ , to  $\text{H}_2$  mass conversion factor,  $\alpha_{\text{CO}}$  (Carilli & Walter 2013; Bolatto et al. 2013), is calibrated to this transition, making observations of CO( $1-0$ ) important for determining the total  $\text{H}_2$  mass content at high- $z$ .

The number of high- $z$  sources with galaxy integrated CO( $1-0$ ) detections is sparse (see Scoville et al. 2017; Carilli & Walter 2013), although it is accumulating (e.g. Carilli et al. 2002; Hainline et al. 2006; Riechers et al. 2011; Harris et al. 2012; Thomson et al. 2012; Riechers et al. 2013; Fu et al. 2013; Aravena et al. 2013; Sharon et al. 2016; Decarli et al. 2016a,b; Huynh et al. 2017), with approximately 60 to date. Resolved imaging of this lowest rotational transition of CO (e.g. Riechers et al. 2011; Lestrade et al. 2011) in high- $z$  SMGs indicates that the total molecular gas can extend up to 30 kpc for merging systems. Only the most active star forming sources with apparent  $L_{\text{IR}} \geq 10^{12-14} L_{\odot}$  at  $z > 1$  can be observed at this fundamental CO rotational transition. These apparent luminosities are often due to strong lensing. The strong lensing effect (usually with magnification factor,  $\mu = 10 - 30X$ ) (e.g. Bussmann et al. 2013, 2015; Geach et al. 2015; Spilker et al. 2016), yields shorter integration times to provide secure detections of the molecular gas in both strongly lensed, intrinsically bright and faint, but highly magnified, normal star-forming systems.

The far-IR/sub-mm *Herschel* Astrophysical Terahertz Large Area Survey (H-ATLAS) (Eales et al. 2010) and the *Herschel* Multi-tiered Extragalactic Survey (HerMES) (Oliver et al. 2012), together covering about  $650 \text{ deg}^2$ , and the  $2500 \text{ deg}^2$  mm South Pole Telescope (*SPT*, Carlstrom et al. 2011) have paved the way forward in discovering a rare population of gravitationally lensed DSFGs (e.g. Negrello et al. 2010; Planck Collaboration et al. 2011; Wardlow et al. 2013; Vieira et al. 2013; Weiß et al. 2013; Negrello et al. 2017), as well as an intrinsically bright, unlensed popula-

tion. Cañameras et al. (2015) and Harrington et al. (2016) have exploited the all-sky sensitivity of *Planck* to find the most luminous high redshift galaxies currently known in the *Planck* era – all of which are gravitationally lensed (also Herranz et al. 2013; Fu et al. 2012; Combes et al. 2012).

Here we present galaxy integrated, CO( $1-0$ ) measurements of seven  $z > 1$  galaxies using the Green Bank Telescope (*GBT*). This is a pilot study for a larger program to identify a large sample of extremely luminous high- $z$  SMGs identified by the all-sky *Planck* survey. In our original pilot study leading to the sample in this work, our goal was to identify sources that have the probability to be gravitationally lensed given their high flux densities in the 3 SPIRE bands of 250, 350, 500  $\mu\text{m}$  (e.g. the  $S_{500}$  or  $S_{350} \geq 100 \text{ mJy}$  Negrello et al. 2010; Ivison et al. 2011). We have previously obtained one  $J_{\text{up}} = 2 - 4$  transition for all seven of the sources presented in this study using the Redshift Search Receiver (RSR) on the *LMT*. The majority of these sources have apparent  $\mu L_{\text{IR}} > 10^{14.0-14.5} L_{\odot}$  making them some of the most luminous sources currently known (Harrington et al. 2016; Cañameras et al. 2015). Our goals in this study are to confirm the *LMT* CO redshift, measure the CO( $1-0$ ) line emission to constrain our estimate of the  $\text{H}_2$  masses and begin analysing the CO spectral line energy distributions (CO SLEDs). In § 2 we review our sample selection and previous observations described in detail in Harrington et al. (2016), and in § 3 we outline our CO( $1-0$ ) observations using the VErSatile GBT Astronomical Spectrometer (VEGAS) instrument on the *GBT*. Measured and derived gas properties using the CO( $1-0$ ) line emission and supplementary *LMT* CO data is found in § 4, followed by a discussion in § 5. Finally, we conclude our study in § 6. We adopt a  $\Lambda$  CDM cosmology with  $H_0 = 70 \text{ kms}^{-1} \text{ Mpc}^{-1}$  with  $\Omega_{\text{m}} = 0.3$ , and  $\Omega_{\Lambda} = 0.7$  throughout this paper.

## 2 SAMPLE

In a search for the most extreme, and thus rare, star-forming galaxies at  $z > 1$ , we exploit the full-sky sub-mm coverage offered by the the *Planck* Catalog of Compact Sources (PCCS). The highest frequency observed by *Planck* (857 GHz / 350  $\mu\text{m}$ ) contains a dataset of  $\sim 24,000$  point source objects (Planck Collaboration XXVIII 2014). From this dataset we limit our searches to point sources at Galactic latitude  $|b| > 30^\circ$  to minimize the Galactic source contamination. This filtered sample is then cross-correlated with the combined catalogs of three *Herschel* large area surveys: *Herschel* Multi-tiered Extragalactic Survey (HerMES, Oliver et al. 2012), *Herschel* Stripe 82 Survey (HerS-82, Viero et al. 2014), and the dedicated *Planck* follow-up *Herschel* DDT “Must-Do” Programme: “The *Herschel* and *Planck* All-Sky Source Snapshot Legacy Survey”.

The details of our selection method can be found in Harrington et al. (2016) for the *Planck* - *Herschel* counterparts with  $S_{350} \geq 100 \text{ mJy}$  in our initial follow-up during the Early Science Campaign 2 for the *LMT*. In brief, we cross-matched *Planck*-*Herschel* counterparts within  $150''$ . In total there were 350 *Herschel* counterparts to 56 *Planck* sources within  $150''$ . The higher spatial resolution of *Herschel* allowed us to pinpoint the position of the *Planck* point sources, enabling follow up studies.

For 8/11 galaxies observed with the *LMT* we detected a single, compact source using the AzTEC 1.1mm camera. Subsequently we detected a strong CO line with the RSR spectrometre. We make use of the 3 SPIRE bands of *Herschel* (250, 350, 500  $\mu\text{m}$ ) and the additional *LMT* observations to derive apparent  $\mu\text{L}_{\text{IR}} > 10^{13.0-14.5}L_{\odot}$  at  $z_{\text{CO}} = 1.33 - 3.26$  (see Table 2). The current sample in this *GBT* study consists of observations of only seven of the original eight targets.

### 3 GBT OBSERVATIONS

Based on our RSR spectroscopy, two of our sources have redshifted CO(1–0) (i.e. rest-frame 115.27 GHz) line emission in the range of the Q band receiver (38.2 – 49.8 GHz) on the *GBT*. The other five sources fall within the K<sub>a</sub> band receiver (26.0 – 40 GHz). We used the low-resolution 1500 MHz bandwidth mode of the backend spectrometre, VEGAS. The raw channel resolution corresponds to 1.465 MHz, or  $\sim 16 \text{ km s}^{-1}$  in K<sub>a</sub> band, using 1024 channels. Observations between February and March, 2016, took place in typical weather conditions. For both Q and K<sub>a</sub> band observations, we used a SubBeamNod procedure, nodding the 8m *GBT* sub-reflector every 6 seconds between each receiver feed for an integration time of four minutes. In most cases, this 4 minute procedure was repeated back-to-back for up to an hour to achieve the ON source integration times presented in Table 1. The atmosphere becomes highly variable at the frequencies within Q and K<sub>a</sub> band, therefore we observed pointing sources roughly every hour. The routine pointing and focus procedures allowed us to assess the best azimuth and elevation corrections, as well as the best focus values for the peak line strength measurements.

After total-power switching for the standard (ON – OFF)/OFF GBTIDL calculations, we include the observatory’s atmospheric model, which tracks zenith opacity as a function of frequency and time. Each scan is corrected for the atmospheric time and frequency variations on the sky, given zenith opacity  $\tau_{\text{sky}}$  and elevation, EL:  $T_{\text{antenna}} = T_{\text{sys}} \times e^{\frac{\tau_{\text{sky}}}{\sin(\text{EL})}} \times \frac{(\text{ON}-\text{OFF})}{\text{OFF}}$ . The elevation ranges for Q and K<sub>a</sub> band spanned 33 – 84 deg and 28 – 73 deg, respectively. The typical  $T_{\text{sys}}$  values ranged from 67-134 K in Q band, and 30 - 45 K in K<sub>a</sub> band. To convert the measured antenna temperature in  $T_A^*$  to flux density we use the calibration factor derived for *GBT*: Q band scales as 1K/1.7 Jy, K<sub>a</sub> band as 1K/1.6Jy.

We used a high-pass filter to remove very low-frequency ripples in the overall baseline without removing the line emission. The width of the high-pass filter was at least twice the expected full-width at half maximum (FWHM) of the CO line based on our *LMT* RSR spectra. We utilised Gaussian smoothing to decrease the resolution by a factor of 4, resulting in a 5.86 MHz ( $\sim 50 \text{ km s}^{-1}$  for K<sub>a</sub>) channel resolution. In this smoothing step, each channel was treated as independent to avoid correlations in the noise of neighboring channels. As the high-pass filter removes the low-frequency ripples, and not the mid-frequency baseline ripples, we then fit and remove a baseline ( $n_{\text{poly}} = 2 - 3$ ) to the emission free regions of the spectra. The resulting spectra can be seen in Fig. 1. We adopt a 30% total uncertainty given a 15-20% flux calibration error, typical 5-10% pointing/focus drifts

and atmospheric losses and a conservative 10-15% for the baseline removal due to the variations across the bandpass at the observed frequencies.

### 4 RESULTS: CO (1 – 0) LINE PROPERTIES

We detect CO(1 – 0) at  $S_{\text{peak}}/N_{\text{channel}} > 7$  from each of our seven targets at the expected redshifts. We first derive the observed central frequency by fitting a single Gaussian to the CO(1 – 0) line emission, confirming the exact redshifts of these *Planck-Herschel* identified galaxies, which had previously been derived using only one CO line from the *LMT*(Tab. 2). The spectroscopic redshifts span from  $1.33 < z < 3.26$ . Our new *GBT* measurements further support our previous redshift determinations from the combination of panchromatic photometry (WISE-11 and 22  $\mu\text{m}$ , *Herschel* SPIRE 250, 350, and 500  $\mu\text{m}$ , AzTEC 1100  $\mu\text{m}$  and NVSS/FIRST radio) and single CO line observations (see Appendix A of (Harrington et al. 2016)).

We find that the CO(1 – 0) lines show nearly identical profiles and widths as the  $J_{\text{up}} = 2 - 4$  CO lines, with FWHM = [375–740  $\text{km s}^{-1}$ ] (see Fig. 1). It is unlikely that there is a significant amount of gas that excites the CO(1 – 0) but not, e.g. the CO(3 – 2). Therefore, the similar line emission FWHM and line profiles suggests that both transitions are tracing co-spatial volumes.

We calculated the line luminosity,  $L'_{\text{CO}(1-0)}$ , using Eq. (3) by Solomon et al. (1997),

$$L'_{\text{CO}} = 3.25 \times 10^7 S_{\text{CO}} \Delta V \nu_{\text{obs}}^{-2} D_L^2 (1+z)^{-3}$$

with  $S_{\text{CO}} \Delta V$  in Jy km s<sup>–1</sup>,  $\nu_{\text{obs}}$  in GHz, and  $D_L$  in Mpc (see Table 3). Since the CO lines are not exactly Gaussian, we also integrated the spectra within  $\pm 1500 \text{ km s}^{-1}$  to compute  $S_{\text{CO}} \Delta V$ . The corresponding Gaussian derived values of  $S_{\text{CO}} \Delta V$  are the same within 1-sigma. Some of the measured apparent  $L'_{\text{CO}}$  are amongst the brightest, if not the brightest, for all  $z > 1$  QSO, SMG, LBG, including the SPT DSFGs (Aravena et al. 2016), as well as  $z < 1$  ULIRGs, nearby spirals, and low- $z$  starburst galaxies (Carilli & Walter 2013). These bright apparent luminosities suggest that our galaxies have been strongly magnified.

### 5 DISCUSSION

#### 5.1 CO Spectral Line Energy Distributions (SLEDs)

In Fig 2 we plot the ratio of the line integrated intensity of the higher-J CO  $S_{\text{CO}} \Delta V$  to our CO(1 – 0)  $S_{\text{CO}} \Delta V$ . All of our galaxies show sub-thermalised excitation conditions. Up to  $J \leq 3$ , we find these values to be consistent with both the lower end of the SMG excitation distribution (Bothwell et al. 2013; Carilli & Walter 2013) and the upper end of the MW (Fixsen et al. 1999). The uncertainty of the MW measurements and the physical intrinsic SMG dispersion overlap for  $J \leq 4$ . Without higher-J CO lines, where SMGs and the MW differ strongly, it is a challenge to disentangle which of these two ISM conditions dominate our galaxies.

**Table 1.** Sources and *GBT* Observations Summary

Source ID	RA	DEC	$\mu L_{IR}^\dagger$	<i>GBT</i> RX	Dates	Int. Time (On-Source)	$\langle T_{sys} \rangle$
	J2000	J2000	( $10^{14} L_\odot$ )		2016	mins	K
PJ142823.9	14h28m23.9s	+35d26m20s	$0.19 \pm 0.04$	Q	2/12;2/19	336	100
PJ160722.6	16h07m22.6s	+73d47m03s	$0.14 \pm 0.03$	Q	2/12;2/19	216	75
PJ105353.0	10h53m53.0s	+05d56m21s	$2.9 \pm 0.4$	K <sub>a</sub>	3/30	100	40
PJ112714.5	11h27m14.5s	+42d28m25s	$1.1 \pm 0.2$	K <sub>a</sub>	3/30	84	40
PJ120207.6	12h02m07.6s	+53d34m39s	$1.4 \pm 0.3$	K <sub>a</sub>	3/30	80	40
PJ132302.9	13h23m02.9s	+55d36m01s	$1.2 \pm 0.2$	K <sub>a</sub>	3/30	96	40
PJ160917.8	16h09m17.8s	+60d45m20s	$2.0 \pm 0.4$	K <sub>a</sub>	3/26	92	35

[1] Q band receiver frequency coverage: 38.2 – 49.8GHz. [2] K<sub>a</sub> band receiver frequency coverage: 26.0 – 40GHz. [3]<sup>†</sup>  $L_{IR}$  is the far-infrared luminosity integrated between 8–1000  $\mu\text{m}$ .

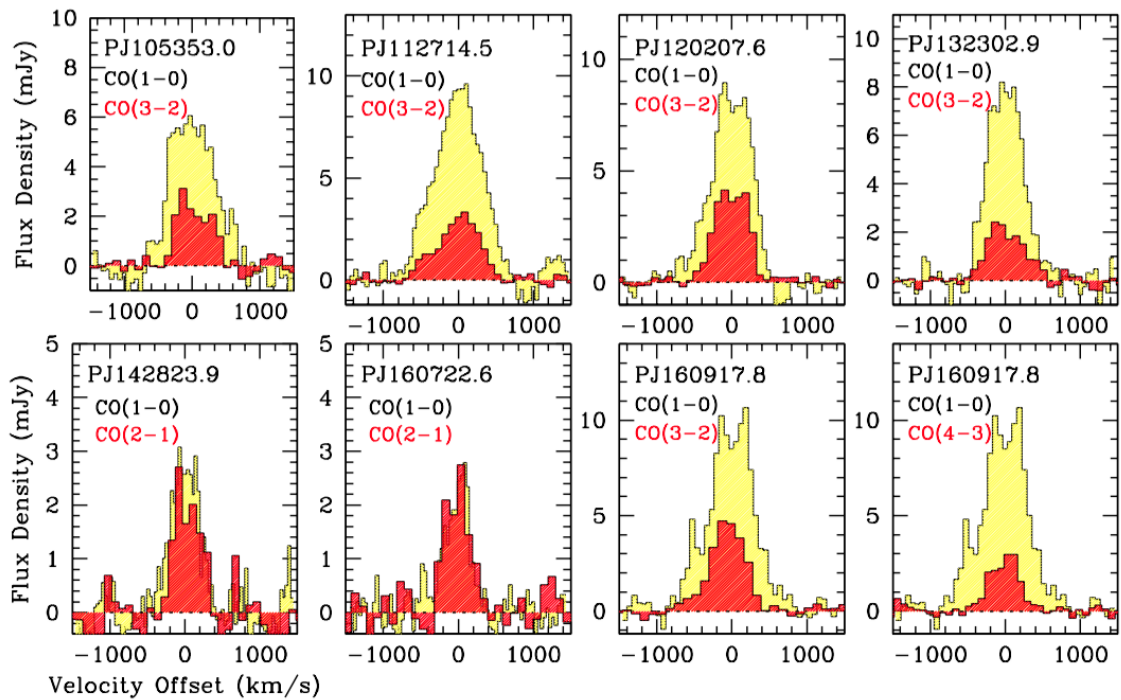


**Figure 1.** The RSR CO spectra (yellow) for all 7 galaxies (Harrington et al. 2016) are scaled by  $J_{up}^2$  and overlaid (red) onto the *GBT* CO spectra (yellow) in this study. The comparable line widths and spectral features are coincident. PJ160918 has both its CO(4–3) and (3–2) lines compared to the (1–0) line emission.

We parametrized these CO SLEDs in terms of brightness temperature, or CO line luminosity, ratios,

$$r_{up,1} = \frac{T_B(J_{upper} > 1)}{T_B(1-0)} = \frac{L'_{CO}(J_{upper} > 1)}{L'_{CO}(1-0)}.$$

For two sources with only  $r_{21}$  we found  $\langle r_{21} \rangle = 0.92$ , while the remaining five sources have  $\langle r_{31} \rangle = 0.34$ . Finally, for the one source with a CO(4–3) line observation, we found  $r_{41} = 0.18$ , similar to what has been reported in Hainline et al. (2006) for an SMG of similar redshift (i.e.  $z \sim 3.3 - 3.5$ ). As noted in (Frayer et al. 2011), there is a wide-range in the observed  $r_{31} = 0.1 - 1$  in the local starburst population. The fact that our galaxies fall in the lower end of the SMG excitation distribution, while being some of the most luminous sources currently known, suggests that they may not be exceptional SMGs, but more strongly magnified sources.

In Harrington et al. (2016) we showed that all of these sources fall within the parameter space for SF powered luminosity (rather than AGN) in a mid-IR to far-IR color-color diagnostic plot (Kirkpatrick et al. 2013). Using their CO SLED we can further rule out the presence of a powerful QSO in our galaxies, as typical QSO host galaxies with powerful AGN activity often exhibit thermalised line ratios out to CO(4–3) (e.g. Riechers et al. 2006; Weiss et al. 2007). However, we caution that most QSO hosts with a good coverage in the CO SLED are strongly lensed objects selected in the optical/NIR. This may result in a bias towards the excitation conditions within the central region. Sharon et al. (2016) show there is a statistical similarity between the  $r_{31}$  values reported for SMGs and AGN in their sample. However, the line ratios in their sample have a global average (AGN and SMG) 3 times higher for  $r_{31}$  (in fact close to thermalised:  $\langle r_{31} \rangle = 0.9$ ) as compared to our



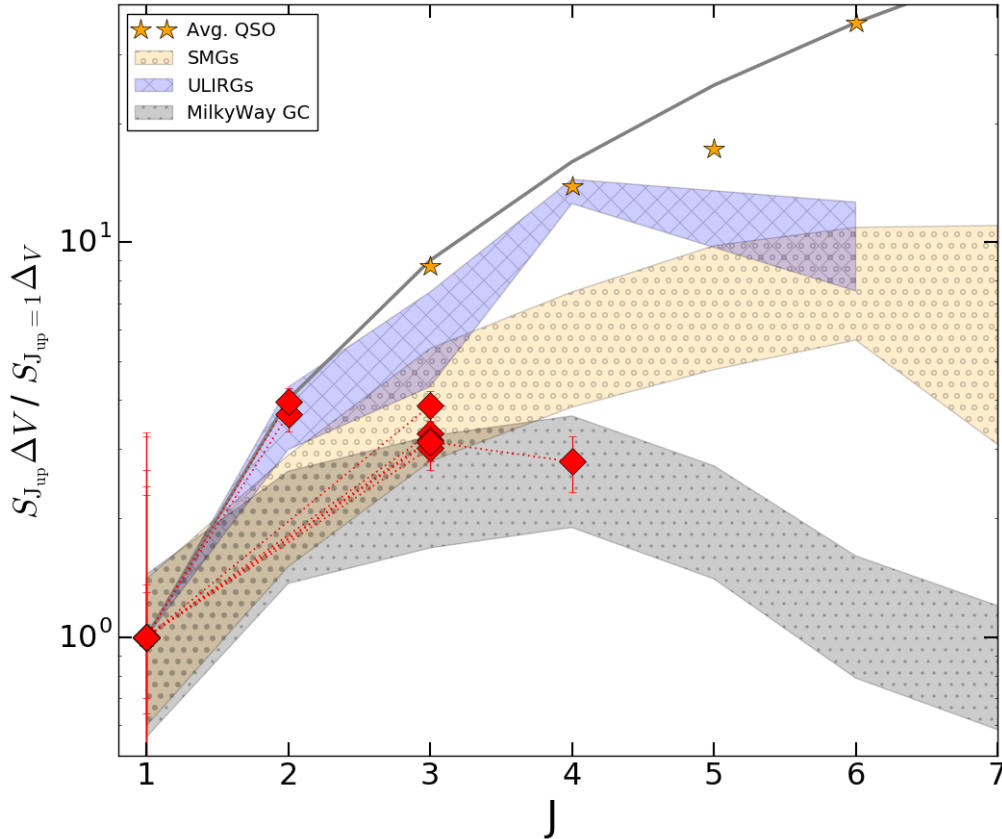


**Figure 2.** Here we plot the velocity-integrated line intensity ratios of  $J_{\text{up}}/J=1$ , normalised to the CO(1–0) derived integrated flux for the current sample. Our seven galaxies (red diamonds) are within the spread for average SMGs (Bothwell et al. 2013) (yellow), and can be compared to the low- $z$  (U)LIRG population (Papadopoulos et al. 2012) (blue), and the Milky Way center (Fixsen et al. 1999) (gray). All regions contain the dispersion between the 25th and 75th percentile of the distribution of the CO(1–0) normalised integrated flux. Yellow stars show the average QSO values out to  $J=6$  (Carilli & Walter 2013).

sources. This suggests that their sample might consist of hybrid SMG/AGN galaxies. Our CO SLEDs are currently limited out to  $J=3$  or 4, therefore we cannot rule out the presence of an AGN.

## 5.2 Ratio of IR Luminosity to CO Line Luminosity

The observable  $\mu L_{\text{IR}}/\mu L'_{\text{CO}(1-0)}$  ratio serves as a proxy for SF efficiency (SFE), and stands independent of the unknown magnification factor<sup>1</sup>. The integrated IR emission (8–1000 $\mu\text{m}$ ) reflects the bulk star-forming activity, while the CO line luminosity indicates the amount of gas supplying the ongoing star formation.

Using the value of this ratio we place our sample in the context of SB versus typical star-forming galaxies at different  $z$ , IR and CO line luminosity (Fig 3; e.g. Genzel et al. 2010). We measure the  $\mu L_{\text{IR}}/\mu L'_{\text{CO}(1-0)}$  ratio as

<sup>1</sup> We assume, without high angular resolution imaging of the two luminosity sources, that the CO(1–0) emitting region and the pervasive dust content are on average co-spatial.

( $58 - 170$ )  $L_{\odot}/(\text{K km s}^{-1} \text{pc}^2)$ , with  $< 110 \pm 22 > L_{\odot}/\text{K km s}^{-1} \text{pc}^2$  (see Fig 3). The average value of our galaxies is closer to  $140 L_{\odot}/(\text{K km s}^{-1} \text{pc}^2)$  observed in SB galaxies, rather than  $30 L_{\odot}/(\text{K km s}^{-1} \text{pc}^2)$  observed in typical star-forming galaxies (Solomon & Vanden Bout 2005; Genzel et al. 2010; Frayer et al. 2011). From this we conclude that the  $L_{\text{IR}}/L'_{\text{CO}(1-0)}$  values obtained for this subset of *Planck-Herschel* sources have enhanced ratios with respect to typical star-forming galaxies, as expected from their large apparent  $L_{\text{IR}}$  (Cañameras et al. 2015; Harrington et al. 2016).

We note that our sample exhibits slightly lower ratios on average compared to both the highly excited system, HFLS-3 ( $z \sim 6$  Riechers et al. 2013), as well as the lensed SPT DSFGs (Aravena et al. 2016) (Fig 3). Roughly half of the strongly lensed, dusty *Herschel* galaxies (Harris et al. 2012) are consistent with our sample and lie within the yellow shaded region for SB systems. In contrast, more than half of the SPT sources have excess  $L_{\text{IR-to-}L'_{\text{CO}(1-0)}}$  Aravena et al. (2016), although the dispersion is similar for both H-ATLAS and SPT samples. Our seven *Planck-Herschel* sample are unusual as they lack a similar dispersion. This may reflect the ability of the all-sky sub-mm sensitivity and coverage of

**Table 2.** Summary of CO(1 – 0) VEGAS Measurements

ID	$\nu_{obs}$ (GHz)	$z_{CO(1-0)}$	$\Delta V$ (km/s)	$S\Delta V^\dagger$ (Jy km/s)	$S_\nu$ Peak (mJy)	$\mu L'_{CO}$ ( $10^{10}$ K km s $^{-1}$ pc $^2$ )
PJ105353.0	28.7712	$3.0053 \pm 0.00016$	$738 \pm 38$	$4.3 \pm 1.3$	$6.2 \pm 1.9$	$170 \pm 60$
PJ112714.5	35.6248	$2.2352 \pm 0.00006$	$736 \pm 20$	$7.4 \pm 2.2$	$9.3 \pm 2.8$	$178 \pm 63$
PJ120207.6	33.4970	$2.442 \pm 0.00007$	$602 \pm 21$	$5.5 \pm 1.7$	$8.9 \pm 2.7$	$154 \pm 55$
PJ132302.9	33.7350	$2.4165 \pm 0.00006$	$540 \pm 17$	$4.7 \pm 1.4$	$8.4 \pm 2.5$	$129 \pm 46$
PJ142823.9	49.5766	$1.3254 \pm 0.00005$	$436 \pm 25$	$1.2 \pm 0.4$	$2.9 \pm 0.9$	$11 \pm 4$
PJ160722.6	46.4115	$1.4838 \pm 0.00006$	$374 \pm 27$	$1.0 \pm 0.3$	$2.4 \pm 0.7$	$12 \pm 4$
PJ160917.8	27.0911	$3.2567 \pm 0.00014$	$705 \pm 31$	$7.6 \pm 2.3$	$9.8 \pm 2.9$	$343 \pm 121$

[1]  $T_A^*$  to flux density using the *GBT*: Q band is 1K/1.7 Jy, Ka band is 1K/1.6 Jy. [2] The reported redshifts correspond to the values obtained after velocity offset corrections. The line widths reported indicate the FWHM values after correcting for the instrumental resolution. This correction was on average less than 1% due to large observed line widths. [3]  $^\dagger$  The integrated value obtained within the interval of  $\pm 1500$  km s $^{-1}$  from the center.

**Table 3.** Gas Properties

ID	$L(IR)/L'_{CO(1-0)}$ $L_\odot/(\text{Kkms}^{-1}\text{pc}^2)$	$r_{up,1}$	$\mu M_{ISM}$ ( $10^{10}M_\odot$ )	$\mu M_{H_2}$ ( $\alpha_{CO}4.3, 0.8$ )( $10^{10} M_\odot$ )	$\tau_{depl-CO}$ ( $\alpha_{CO}4.3, 0.8$ ) (Myr)	$\tau_{depl-ISM}$ (Myr)
PJ105353.0	$170 \pm 65$	$0.36 \pm 0.13[r_{31}]$	$624 \pm 156$	$[732, 136] \pm [259, 54]$	$[239, 44]$	203
PJ112714.5	$62 \pm 25$	$0.29 \pm 0.10[r_{31}]$	$160 \pm 40$	$[764, 142] \pm [270, 27]$	$[636, 118]$	133
PJ120207.6	$91 \pm 38$	$0.4 \pm 0.14[r_{31}]$	$452 \pm 113$	$[663, 123] \pm [234, 30]$	$[442, 82]$	302
PJ132302.9	$93 \pm 36$	$0.31 \pm 0.11[r_{31}]$	$215 \pm 54$	$[557, 103] \pm [196, 23]$	$[425, 79]$	164
PJ142823.9	$168 \pm 69$	$0.88 \pm 0.36[r_{21}]$	$97 \pm 24$	$[49, 9] \pm [17, 4]$	$[228, 42]$	452
PJ160722.6	$121 \pm 50$	$0.95 \pm 0.38[r_{21}]$	$52 \pm 13$	$[50, 9] \pm [18, 5]$	$[331, 62]$	344
PJ160917.8	$58 \pm 24$	$0.35 \pm 0.13[r_{31}]$	$465 \pm 116$	$[1473, 274] \pm [521, 85]$	$[694, 129]$	219
PJ160917.8	–	$0.18 \pm 0.06[r_{41}]$	–	–	–	–

[1] Unknown lensing amplification  $\mu$  is reflected in the derived CO luminosity and  $H_2$  mass. ISM masses were calculated following [Scoville et al. \(2016\)](#), scaled to our AzTEC 1.1mm photometry with a fixed dust temperature of 25 K.

the *Planck* survey in detecting the rare galaxies that are, on average, more strongly lensed than the similarly selected H-ATLAS sample.

While the SPT lensed galaxies are a similar population at high- $z$  with comparable  $L_{IR}$ , due to different selection methods (350  $\mu\text{m}$  versus mm), the average redshift of their sample is significantly shifted towards a higher value compared to our sample:  $\langle z \rangle = 3.9$  and  $\langle z \rangle = 2.3$ , respectively. At such a high redshift,  $z \sim 4$ , a MW type galaxy would be subject to non-negligible dust heating due to the CMB ([da Cunha et al. 2013](#)), and may contribute to the higher  $L_{IR}$ -to- $L'_{CO(1-0)}$  values observed in the SPT sample. At  $z \sim 4$ , the CMB temperature is also a sufficient background to radiatively excite the cool reservoirs of CO, particularly the  $J=1 \rightarrow 0$  ground state rotational transition, resulting in a dimming of the observed CO line emission. Because (sub)-mm flux measurements are made against the CMB, the contrast in the CO (1–0) line integrated intensity via collisional excitation (typically with  $H_2$  molecules), compared with the radiatively excited CO gas from the CMB background becomes more severe beyond  $z = 4$ . About 80% of the CO (1–0) emission can be recovered against the CMB at  $z = 2 - 3$ , but only 50-60% just beyond  $z = 4$  if there would be a gas kinetic temperature of 40 K ([da Cunha et al. 2013](#)).

We caution that the effects of the CMB alone cannot account for the differences observed in these luminosity-luminosity ratios, as the H-ATLAS and SPT sample have

a similar spread in their  $L_{IR}$ -to- $L'_{CO(1-0)}$  values. The similar redshift range of the 12 H-ATLAS sample compared to the sample of 7 *Planck-Herschel* galaxies in this study reveals that the CMB effects cannot explain this offset. The excitation conditions of a multi-phase, multiple gas component ISM are also expected to change for each galaxy. One would expect that the density and kinetic temperature of the CO (1 – 0) emitting gas (and the gradients across the galaxy) to factor into the total attenuation of the CO (1 – 0) line emission ([Tunnard & Greve 2016, 2017](#)) and any self-shielding. As the intense star-forming conditions during the redshifts indicated in these three samples (SPT, H-ATLAS, *Planck-Herschel*) will give rise to a dynamic set of ISM conditions, these varying gas excitation conditions will therefore have non-negligible effects in the observed  $L_{IR}$ -to- $L'_{CO(1-0)}$  values.

### 5.3 Total gas mass from $L'_{CO(1-0)}$

CO is the second most abundant molecule in the ISM after the highly abundant molecular hydrogen,  $H_2$ , and the CO(1 – 0) line emission is the most direct proxy for  $H_2$  as it traces even the most diffuse gas. Our galaxy integrated CO(1 – 0) line luminosity is converted to a total molecular gas mass assuming an  $\alpha_{CO}$  conversion factor (see review by [Bolatto et al. 2013](#)). It is common to use a standard ULIRG conversion, i.e.  $\alpha_{CO} = 0.8$ , for star bursting SMG/DSFGs at high- $z$ , although we reference a standard

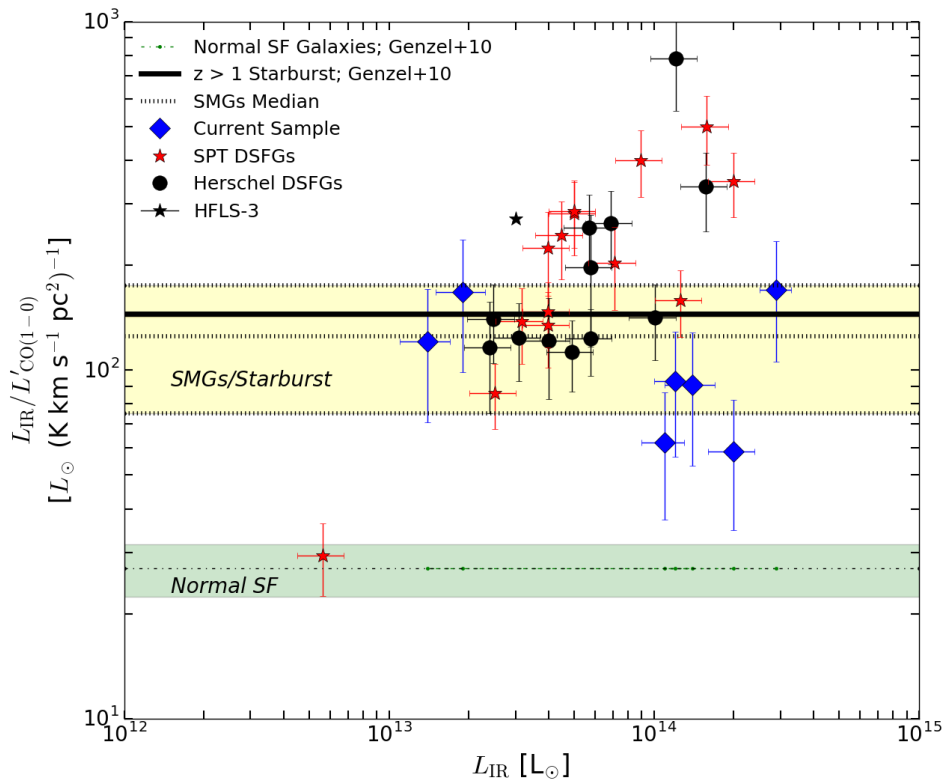


**Figure 3.** Here we present the  $L_{\text{IR}}/L'_{\text{CO}(1-0)}$  ratios of our sample compared with known, lensed *Herschel* and SPT DSFGs (Harris et al. 2012; Aravena et al. 2016), the highly excited HFLS-3 (Riechers et al. 2013) and the median for all SMGs ( $125 \pm 50 L_{\odot}/\text{Kkm s}^{-1}\text{pc}^{-2}$ ) compiled in the literature by Frayer et al. (2011) (shaded yellow). We plot  $2\sigma$  boundaries taken from Genzel et al. (2010) for starburst ( $140 L_{\odot}/\text{Kkm s}^{-1}\text{pc}^{-2}$ ) and typical star-forming galaxies ( $30 L_{\odot}/\text{Kkm s}^{-1}\text{pc}^{-2}$ ). The average for our seven targets in this study is  $110 \pm 22 L_{\odot}/(\text{Kkm s}^{-1}\text{pc}^2)$ .

Galactic value in Table 3. The similarity of the  $L_{\text{IR}}/L'_{\text{CO}(1-0)}$  ratios observed in our sample and those of local ULIRGs seems to further support the use of a starburst-like  $\alpha_{\text{CO}}$  conversion factor, even if the centrally compact, concentrated nuclei in local ULIRGs may not be representative of the entire ISM environments in our galaxies. We found  $\mu M_{\text{H}_2} = (0.9 - 27.4) \times 10^{11} M_{\odot} (\alpha_{\text{CO}}/0.8)$ , which are amongst the largest apparent gas contents measured at high- $z$ , even if a lensed magnification of an order of magnitude is taken into account (see Carilli & Walter 2013).

We also compare our CO-based gas mass to the ISM gas mass estimates using the empirical calibration from measured rest-frame dust continuum (e.g. Scoville et al. 2016, 2017). Using our AzTEC 1.1mm photometry ( $\nu_{\text{obs}} = 272 \text{ GHz} \rightarrow \text{rest-frame } 250\text{-}470\mu\text{m}$ ), we compute the ISM mass using Eq. 14 of Scoville et al. (2017). The ISM masses we report scatter predictably around the values obtained from a ULIRG or Galactic conversion factor, suggesting that the value for  $\alpha_{\text{CO}}$  varies intrinsically from galaxy to galaxy. Later in § 5.5 we will revisit this empirical calibration to compare the CO line luminosity to the specific luminosity at rest-frame  $850\mu\text{m}$ .

#### 5.4 Gas Depletion Time Scales

The amount of time for a galaxy to consume its total molecular gas, given its current galaxy integrated star formation rate, is its so-called depletion time, or gas consumption time scale,  $\tau_{\text{depl}} = \mu M_{\text{H}_2} / \mu SFR$ . This inverse SFE reflects the nature of the SF activity of a galaxy, and is a measure that stands independent of the magnification factor in the same way for the  $L_{\text{IR}}\text{-to-CO}(1-0)$  line luminosity ratios above.

To derive our SFR estimates we used the integrated 8-1000 $\mu\text{m}$  SED and the empirical calibration (Kennicutt 1998) to convert  $L_{\text{IR}}$  to SFR – adopting a Kroupa IMF. The values we obtain are, uncorrected for magnification amplification,  $\sim 1500 - 30700 M_{\odot}\text{yr}^{-1}$  (Harrington et al. 2016). Combined with the CO-based gas masses reported in § 5.3, this suggests a depletion time scale of  $\tau_{\text{depl}} \sim 80 \text{ Myr}$ . These actively evolving galaxies represent a special mode of rapid starburst activity. This is consistent with short gas depletion times observed on the order of  $\tau_{\text{depl}} = 10 - 100 \text{ Myr}$  (e.g. Genzel et al. 2015; Béthermin et al. 2016; Aravena et al. 2016; Scoville et al. 2016), and also with typical galaxy-galaxy crossing time ( $\sim 100 \text{ Myr}$ ; (Scoville et al. 2016)). The rapid  $\tau_{\text{depl}}$  in

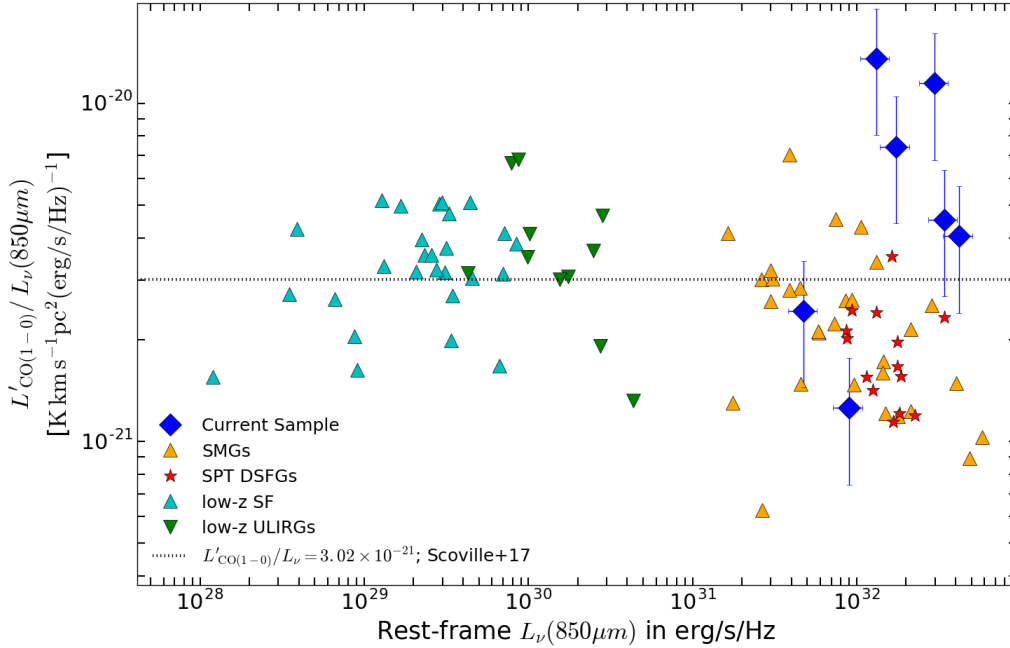


**Figure 4.** We compare our measured  $L'_{CO(1-0)}$  to rest-frame  $L_\nu(353GHz/850\mu m)$  in our sample to the low- $z$  star-forming galaxies (Dale et al. 2012; Young et al. 1995), local ULIRGs (Mentuch Cooper et al. 2012; Chu et al. 2017; Sanders et al. 1989, 1991; Solomon et al. 1997),  $z \sim 2$  SMGs (Greve et al. 2003; Harris et al. 2010; Ivison et al. 2011; Carilli et al. 2011; Harris et al. 2012; Riechers et al. 2011; Lestrade et al. 2011; Thomson et al. 2012; Ivison et al. 2013; Fu et al. 2013; Aravena et al. 2013; Thomson et al. 2015), and lensed SPT galaxies (Aravena et al. 2016) with global measurements of CO(1–0) – or CO(2–1) for some SPT sources, where we used  $r_{21} = 0.9$  when applicable. We overplot the best fit linear relation from Scoville et al. (2017):  $L'_{CO(1-0)} = 3.02 \times 10^{-21} L_{\nu 850}$ .

these galaxies at high- $z$  rival the  $\tau_{\text{depl}} = 2.2$  Gyr timescales for normal star-forming galaxies at  $z = 0$  (Leroy et al. 2013).

### 5.5 Global Gas to Dust Comparison

The ratio of measured  $L'_{CO(1-0)}$  to rest-frame specific luminosity at  $850\mu m$  serves as a foundation for converting the optically thin Rayleigh-Jeans dust continuum, observed in the (sub)-mm, into total ISM mass (Scoville et al. 2014, 2016, 2017). To infer the rest-frame  $850\mu m$  of our galaxies, and thus to compare them to the empirical relation, we use the far-IR SED model fit procedure described by Harrington et al. (2016), fitting the *Herschel* SPIRE 250–500  $\mu m$  and AzTEC 1.1mm photometry with a modified blackbody (Eq. 14 Yun & Carilli 2002) (Fig. 4). Several of  $z \sim 2$ –3 galaxies lie above the empirical calibration obtained by Scoville et al. (2017). In Scoville et al. (2017) the SED analyses was redone using the published sub-mm photometry and CO(1–0) line emission for the 30 normal low- $z$  star-forming galaxies (Dale et al. 2012; Young et al. 1995), 12 low- $z$  ULIRGs (Mentuch Cooper et al. 2012; Chu et al. 2017; Sanders et al. 1989, 1991; Solomon et al. 1997), and 30 SMGs (Greve et al. 2003; Harris et al. 2010; Ivison et al. 2011; Carilli et al. 2011; Harris et al. 2012; Riechers et al. 2011; Lestrade et al. 2011; Thomson et al. 2012; Ivison et al. 2013; Fu et al. 2013; Aravena et al. 2013; Thomson et al. 2015) at comparable redshifts to our sample. This empirical relation, based primarily on galaxies with solar metallicities, was recently validated using

$\sim 70$  main-sequence, low- $z$  star-forming galaxies (Hughes et al. 2017). Without optical or FIR fine-structure emission lines we cannot directly constrain the metallicities of our sample. However, we do not expect these galaxies to have sub-solar metallicities given their large apparent dust masses ( $\mu M_d = [0.1 - 2] \times 10^{10} M_\odot$ ) and given the empirical mass-metallicity relationship out to high- $z$  (Geach et al. 2011; Saintonge et al. 2016).

The SMG/DSFG population predominantly falls below the 1:1 relation, making our small sample the first to populate the upper envelope—which corresponds to a higher amount of observed CO gas per unit  $850\mu m$  dust emission. The highest value of  $L'_{CO}/L_{850}$  observed in the SMG population compiled by Scoville et al. (2017) is the  $350\mu m$  selected source in Ivison et al. (2011). Two of our galaxies are above the observed scatter, while three of our galaxies exhibit extreme CO luminosities compared to their rest-frame dust luminosity. A larger sample is undoubtedly required to further unveil if, as suggested by our sample, there is a larger intrinsic scatter at high- $z$ , particularly at  $\log(L'_{CO(1-0)}) > 10.5$   $K \text{ km s}^{-1} \text{ pc}^2$  and  $\log(L_{\nu 850}) > 31.5$   $\text{ergs}^{-1} \text{ Hz}^{-1}$ . To compare to the SPT-DSFGs with  $J \leq 2$  CO line detections (Aravena et al. 2016), we take their 18 galaxies with consistent sampling of 0.25–1.4mm photometry, similar to our 0.25–1.1mm data, and fit their FIR-mm SEDs as described above. Those SPT galaxies with only CO(2–1) were converted to  $L'_{CO(1-0)}$  using an  $r_{21} = 0.9$ .

The relatively high  $L'_{CO}/L_{850}$  ratios observed in our



galaxies indicate larger gas-to-dust mass (GDMR) ratios than observed in previous samples (Fig. 4). Converting the AzTEC 1.1mm continuum measurement into dust mass, assuming  $T_d = 25\text{K}$ , we found GDMRs in the range [40-200] using the CO-based gas mass ( $\alpha_{\text{CO}} = 0.8$ ), compared with the average GDMR of  $\sim 230$  from the 1.1mm derived ISM mass (Scoville et al. 2017). This range is both consistent, though slightly larger, than observed in local galaxies with solar metallicities (Leroy et al. 2011; Draine et al. 2007). Assuming instead a Galactic  $\alpha_{\text{CO}} = 4.3$ , we would infer extremely high GDMRs (up to 1100), only observed in local, greatly metal-poor dwarf galaxies, e.g., the blue compact dwarf, I Zwicky 18, with 1/50 solar metallicity (Annibali et al. 2015). The assumption of  $\alpha_{\text{CO}}$ , as well as the choice of dust temperature in the ISM mass calculations ultimately determines the derived GDMRs.

## 6 CONCLUSIONS

Using VEGAS on the *GBT*, we have successfully measured the CO(1–0) line emission for seven of the most gas-rich SMGs/DSFGs studied to date. The key results of this study can be summarised as:

- We have confirmed the previously determined spectroscopic redshifts reported by Harrington et al. (2016)
- The linewidths/profiles for the low-J RSR and CO(1–0) VEGAS measurements are nearly identical; therefore the emitting regions are likely co-spatial, with  $\langle \text{FWHM} \rangle = 590 \text{ km s}^{-1}$ ,
- The CO SLEDs of the galaxies in our sample are indicative of a gas component with sub-thermal excitation conditions: CO line luminosity ratios of  $\langle r_{21} \rangle = 0.92$  (2 sources),  $\langle r_{31} \rangle = 0.34$  (5 sources), and  $r_{41} = 0.18$  (1 source)
- We find enhanced  $L_{\text{IR}}/L'_{\text{CO}(1-0)}$  ratios with respect to normal star-forming systems, as we report an average value of  $110 \pm 22 L_{\odot}/(\text{K km s}^{-1} \text{ pc}^2)$ , comparable to the median of other well studied SMGs.

With the CO(1–0) line emission we place tight constraints on the total molecular gas mass, and allow future CO SLED analyses to benefit from having the fundamental rotational transition observed. The large gas masses obtained are  $\mu M_{\text{H}_2} = (0.9–27) \times 10^{11} (\alpha_{\text{CO}}/0.8) M_{\odot}$ . The average gas depletion time we find is  $\tau_{\text{depl}} \sim 80 \text{ Myr}$ . These extremely luminous IR galaxies (with  $L_{\text{IR}} \geq 10^{13-14} L_{\odot}$ ) exhibit rapid depletion timescales, and we are likely capturing this light from a relatively short-lived starburst episode.

## 7 ACKNOWLEDGEMENTS

The quality of this manuscript, and the scientific considerations, have been improved significantly after discussions with N. Scoville, L. Liang and M. Sargent. All authors would like to thank the referee for their kind considerations of how this paper can be developed so as to make its most useful contribution to the field. KCH and DB would like to also thank Karen O’Neil and Toney Minter for organizing, and supporting our travel to, the first *GBT* remote observing school at the Green Bank Telescope. KCH would like to express great thanks to D. Frayer and all of the control room operators

(specifically Amber and Donna) for making the observations run as smooth as possible. The Green Bank Observatory is a facility of the National Science Foundation operated under cooperative agreement with Associated Universities, Inc. KCH and DB heartily acknowledge our financial support granted to us by UMass Amherst’s Astronomy Department, while KCH much appreciated the ongoing support from the UMass Amherst Commonwealth Honors College Research Grant which led to the travel to the *GBT* remote observing school in January, 2016. KCH, AK and EFJA acknowledge the support by the Collaborative Research Center (CRC) 956, subproject A1, funded by the Deutsche Forschungsgemeinschaft (DFG). KCH acknowledges the financial support from the CRC-956 student exchange program. This opportunity has enabled KCH to engage in useful discussions and supervision with D. Riechers, who provided strong guidance in the final stages of this manuscript. Support for BM was provided by the DFG priority program 1573 ‘The physics of the interstellar medium’. KCH is a member of, and receives financial support for his research by, the International Max-Planck research school for Astronomy and Astrophysics at the Universities of Bonn and Cologne and through the Max-Planck-Institut für Radioastronomie.

## REFERENCES

- Annibali F., Cignoni M., Tosi M., van der Marel R. P., Aloisi A., Fiorentino G., 2015, *Mem. Soc. Astron. Italiana*, **86**, 294
- Aravena M., et al., 2013, *MNRAS*, **433**, 498
- Aravena M., et al., 2016, *MNRAS*, **457**, 4406
- Baugh C. M., Lacey C. G., Frenk C. S., Granato G. L., Silva L., Bressan A., Benson A. J., Cole S., 2005, *MNRAS*, **356**, 1191
- B  thermin M., et al., 2016, *A&A*, **586**, L7
- Bolatto A. D., Wolfire M., Leroy A. K., 2013, *ARA&A*, **51**, 207
- Bothwell M. S., et al., 2013, *MNRAS*, **429**, 3047
- Bussmann R. S., et al., 2013, *ApJ*, **779**, 25
- Bussmann R. S., et al., 2015, *ApJ*, **812**, 43
- Ca  nmeras R., et al., 2015, *A&A*, **581**, A105
- Carilli C. L., Walter F., 2013, *ARA&A*, **51**, 105
- Carilli C. L., et al., 2002, *ApJ*, **575**, 145
- Carilli C. L., Hodge J., Walter F., Riechers D., Daddi E., Danerbauer H., Morrison G. E., 2011, *ApJ*, **739**, L33
- Carlstrom J. E., et al., 2011, *PASP*, **123**, 568
- Casey C. M., Narayanan D., Cooray A., 2014, *Physics Reports*, **541**, 45
- Chu J. K., et al., 2017, *ApJS*, **229**, 25
- Combes F., et al., 2012, *A&A*, **538**, L4
- Dale D. A., et al., 2012, *ApJ*, **745**, 95
- Decarli R., et al., 2016a, preprint, ([arXiv:1607.06770](https://arxiv.org/abs/1607.06770))
- Decarli R., et al., 2016b, *ApJ*, **833**, 70
- Draine B. T., et al., 2007, *ApJ*, **663**, 866
- Eales S., et al., 2010, *PASP*, **122**, 499
- Efstathiou A., Rowan-Robinson M., Siebenmorgen R., 2000, *MNRAS*, **313**, 734
- Fixsen D. J., Bennett C. L., Mather J. C., 1999, *ApJ*, **526**, 207
- Frayer D. T., et al., 2011, *ApJ*, **726**, L22
- Fu H., Jullo E., Cooray A., Bussmann R. S., Ivison R. J., et al., 2012, *ApJ*, **753**, 134
- Fu H., et al., 2013, *Nature*, **498**, 338
- Geach J. E., Smail I., Moran S. M., MacArthur L. A., Lagos C. d. P., Edge A. C., 2011, *ApJ*, **730**, L19
- Geach J. E., et al., 2015, *MNRAS*, **452**, 502
- Genzel R., et al., 2010, *MNRAS*, **407**, 2091
- Genzel R., et al., 2015, *ApJ*, **800**, 20
- Greve T. R., Ivison R. J., Papadopoulos P. P., 2003, *ApJ*, **599**, 839

- Hainline L. J., Blain A. W., Greve T. R., Chapman S. C., Smail I., Ivison R. J., 2006, *ApJ*, **650**, 614
- Harrington K. C., et al., 2016, *MNRAS*, **458**, 4383
- Harris A. I., Baker A. J., Zonak S. G., Sharon C. E., Genzel R., Rauch K., Watts G., Creager R., 2010, *ApJ*, **723**, 1139
- Harris A. I., et al., 2012, *ApJ*, **752**, 152
- Hayward C. C., Jonsson P., Kereš D., Magnelli B., Hernquist L., Cox T. J., 2012, *MNRAS*, **424**, 951
- Hernquist L., 1992, in Filippenko A. V., ed., *Astronomical Society of the Pacific Conference Series Vol. 31, Relationships Between Active Galactic Nuclei and Starburst Galaxies*. p. 351
- Herranz D., et al., 2013, *A&A*, **549**, A31
- Hughes T. M., et al., 2017, preprint, ([arXiv:1702.07350](https://arxiv.org/abs/1702.07350))
- Huyh M. T., et al., 2017, *MNRAS*, **467**, 1222
- Ivison R. J., Papadopoulos P. P., Smail I., Greve T. R., Thomson A. P., Xilouris E. M., Chapman S. C., 2011, *MNRAS*, **412**, 1913
- Ivison R. J., et al., 2013, *ApJ*, **772**, 137
- Johnson S. P., et al., 2013, *MNRAS*, **431**, 662
- Kennicutt J. R. C., 1998, *ARA&A*, **36**, 189
- Kereš D., Katz N., Weinberg D. H., Davé R., 2005, *MNRAS*, **363**, 2
- Kirkpatrick A., et al., 2013, *ApJ*, **763**, 123
- Leroy A. K., et al., 2011, *ApJ*, **737**, 12
- Leroy A. K., et al., 2013, *AJ*, **146**, 19
- Lestrade J.-F., Carilli C. L., Thanjavur K., Kneib J.-P., Riechers D. A., Bertoldi F., Walter F., Omont A., 2011, *ApJ*, **739**, L30
- Madau and Dickinson, 2014, *ARA&A*, **52**, 415
- Mentuch Cooper E., et al., 2012, *ApJ*, **755**, 165
- Narayanan D., et al., 2015, *Nature*, **525**, 496
- Negrello M., Hopwood R., De Zotti G., Cooray A., Verma A., et al., 2010, *Science*, **330**, 800
- Negrello M., et al., 2017, *MNRAS*, **465**, 3558
- Oliver S. J., et al., 2012, *MNRAS*, **424**, 1614
- Papadopoulos P. P., van der Werf P. P., Xilouris E. M., Isaak K. G., Gao Y., Mühle S., 2012, *MNRAS*, **426**, 2601
- Planck Collaboration XXVIII 2014, *A&A*, **571**, A28
- Planck Collaboration et al., 2011, *A&A*, **536**, A7
- Riechers D. A., et al., 2006, *ApJ*, **650**, 604
- Riechers D. A., Hodge J., Walter F., Carilli C. L., Bertoldi F., 2011, *ApJ*, **739**, L31
- Riechers D. A., et al., 2013, *Nature*, **496**, 329
- Saintonge A., et al., 2016, *MNRAS*, **462**, 1749
- Sanders D. B., Scoville N. Z., Zensus A., Soifer B. T., Wilson T. L., Zylka R., Steppe H., 1989, *A&A*, **213**, L5
- Sanders D. B., Scoville N. Z., Soifer B. T., 1991, *ApJ*, **370**, 158
- Scoville N., et al., 2014, *ApJ*, **783**, 84
- Scoville N., et al., 2016, *ApJ*, **824**, 63
- Scoville N., et al., 2017, *ApJ*, **837**, 150
- Sharon C. E., Riechers D. A., Hodge J., Carilli C. L., Walter F., Weiß A., Knudsen K. K., Wagg J., 2016, *ApJ*, **827**, 18
- Solomon P. M., Vanden Bout P. A., 2005, *ARA&A*, **43**, 677
- Solomon P. M., Downes D., Radford S. J. E., Barrett J. W., 1997, *ApJ*, **478**, 144
- Spilker J. S., et al., 2016, *ApJ*, **826**, 112
- Swinbank A. M., et al., 2008, *MNRAS*, **391**, 420
- Thomson A. P., et al., 2012, *MNRAS*, **425**, 2203
- Thomson A. P., Ivison R. J., Owen F. N., Danielson A. L. R., Swinbank A. M., Smail I., 2015, *MNRAS*, **448**, 1874
- Tunnard R., Greve T. R., 2016, *ApJ*, **819**, 161
- Tunnard R., Greve T. R., 2017, *ApJ*, **849**, 37
- Vieira J. D., et al., 2013, *Nature*, **495**, 344
- Viero M. P., et al., 2014, *ApJS*, **210**, 22
- Wardlow J. L., et al., 2013, *ApJ*, **762**, 59
- Weiss A., Downes D., Walter F., Henkel C., 2007, in Baker A. J., Glenn J., Harris A. I., Mangum J. G., Yun M. S., eds, *Astronomical Society of the Pacific Conference Series Vol. 375, From Z-Machines to ALMA: (Sub)Millimeter Spectroscopy of Galaxies*. pp 25–
- Weiß A., et al., 2013, *ApJ*, **767**, 88
- Young J. S., et al., 1995, *ApJS*, **98**, 219
- Yun M. S., Carilli C. L., 2002, *ApJ*, **568**, 88
- da Cunha E., et al., 2013, *ApJ*, **766**, 13